CFSRC COLLOQUIUM

Proceedings of the Cold-Formed Steel Research Consortium Colloquium
20-22 October 2020 (cfsrc.org)

Buckling Analysis, Structural Behavior and Strength of Distortional-Global Interaction in Cold-Formed Steel Lipped Channel Columns

Joao Alfredo de Lazzari[1], Eduardo de Miranda Batista[2]

Abstract

Cold-formed steel members are composed of thin-walled sections, forming very slender structural systems easily susceptible to buckling. This unique characteristic obligates designers to deal with the complexity of the phenomenon and requires research development to allow structural solution with simple equations. In terms of design procedures, these structural design equations are still under constant adjustments. The goal of the present research is the distortional-global (DG) buckling interaction of cold-formed steel lipped channel columns, in its buckling structural behavior and strength nature. Recent studies on this topic have been presented in the literature, however, the DG interaction still needs investigation in order to accomplish the definition of safe design procedures. For the buckling analysis, the Finite Strip Method-based software FStr Computer Application is developed, in order to perform the elastic buckling analysis, mainly focused in a simple and accessible graphical user interface. The FStr computational program generates the modal shapes which are inserted as the initial geometric imperfections in the finite element software ANSYS, in order to perform geometric and material nonlinear analysis. The buckling modes combination as initial imperfection helps to understand the DG buckling interaction, which is not feasible to predict with the first order elastic buckling analysis. It was observed that the global buckling strength equations from the Direct Strength Method (the most widely applied design method for cold-formed steel structures included in recognized design standards, attributable to its simplicity and accuracy in identifying the ultimate load of cold-formed steel members), have shown good agreement with the geometric and material nonlinear analysis results of columns of the present research, indicating a plausible design solution for the case of DG buckling interaction of cold-formed steel lipped channel columns. As suggestions for future work, the authors recommend a more robust parametric study, including: (i) new types of cross-sections geometries, (ii) other type of parametric analysis, and (iii) experimental tests results. Additionally, the authors are also planning several updates for the FStr Computer Application.

Key Words: Cold-formed Steel, Buckling Modes Interaction, Finite Strip Method, Lipped Channel Columns.

1. Introduction

The major task of structural engineers is to design low-cost and safe solutions. Thus, saving weight on the structure will lead to solution with less material consumption and, consequently, a better economical option. Under these circumstances, light steel construction enables cost savings within the superstructure as well as in the substructure and foundation. Choosing thin-walled steel members may be a frequent option due to less material consumption, engineering design and architectural concepts. However, light gauge steel members are slender structures, which present additional stability problems, Batista [1].

In terms of design procedures, these structural design equations are still under constant adjustments. The current codes, Brazilian standard ABNT NBR 14762:2010 [2], Australian/New Zealand code AS/NZS 4600 [3] and North-American standard AISI S100-16 [4], have been changing their designing approaches over the past decades. The need of constant modifications on the design procedures, due to the semi-empirical procedures, obliges laboratory experimental campaigns combined with accurate numerical solutions in order to calibrate the equations and procedures.

The most widely applied design method for cold-formed steel structures is the Direct Strength Method, DSM. The first proposal for the DSM was published by Schafer and

[1] Graduate Research Assistant, Civil Engineering Program, COPPE, Federal University of Rio de Janeiro, Brazil, joaoadelazzari@outlook.com.br
[2] Full Professor, Civil Engineering Program, COPPE, Federal University of Rio de Janeiro, Brazil, batista@coc.ufrj.br

Peköz [5], based on the original idea of Hancock *et al.* [6]. This method became so widespread attributable to its simplicity and accuracy in identifying the ultimate load of cold-formed steel, CFS, members. However, the available equations of the method have some breaches. Up until now, the current standards (*e.g.* ABNT NBR 14762:2010 [2], AS/NZS 4600 [3] and AISI S100-16 [4]), adopt the direct strength method considering only local, distortional, global and local-global buckling interaction design procedure. Nevertheless, further coupled buckling phenomena are not addressed, *i.e.* local-distortional, distortional-global, local-distortional-global and global-global buckling interaction. The motivation of this research is to comprehend the distortional-global interaction in order to propose a new direct strength method solution that contemplate the coupled phenomenon.

The buckling coupled phenomena must be considered for the structural design, since the modal interaction may conduct to reduction of the strength capacity, usually recognized as erosion of the limit load, as reported by Batista [1]. The Local-Global, LG, interaction is already in the standards for hot-rolled and CFS members in the effective section method by Batista [7], as well as in the direct strength method (DSM) by Schafer [8] & [9]. Up to now, it is the most frequently adopted method for designing CFS structures.

Many research efforts have been developed since the early investigations devoted to the buckling modes interaction. Recently, other buckling mode interaction in CFS lipped channel sections have been under investigation these last decades: local-distortional, LD (*e.g.* Chen *et al.* [10], Martins *et al.* [11], and Matsubara *et al.* [12]), distortional-global, DG (*e.g.* Dinis and Camotim [13] and Martins *et al.* [14]) and local-distortional-global, LDG (*e.g.* Santos *et al.* [15] and Matsubara and Batista [16]). One may find recent results indicating robust conclusions and design propositions to handle these particular coupled phenomena cases. Anyway, the challenge is to define as simple as possible rules with clear physical meaningful and avoiding intricate blank box solution.

The purpose of this work is to investigate the distortional-global coupled phenomenon in cold-formed steel lipped channel columns. More specifically, it is focused on the phenomenon behavior and the column strength under different types of initial imperfections and the column slenderness, which can be achieved with appropriate variations of the columns' length and steel yield stress. Additionally, the obtained results of the strength of the columns under DG buckling interaction are compared with design procedures found in the literature.

2. Elastic Buckling Analysis: Matrix Formulation of the Finite Strip Method

The finite strip method formulation for structural buckling analysis is based on the classical plate theory assumptions, which is described in detail by Timoshenko and Woinowsky-Krieger [17]. For this work, the computational matrix formulation is presented, for an elastic buckling analysis, with the main reference by Cheung [18]. According to Cheung [18], the first paper that presented the finite strip method was from Cheung [19] for a simply supported plate-bending rectangular strip. Later, in Cheung [20] the formulation was generalized, including other end-conditions. Some other sources are also used in the present work – *i.e.* Bradford and Azhari [21], Li and Shafer [22], Schafer [23] and Li [24].

The strip element is a lower order rectangular strip with two nodal lines (LO2). For each strip, the membrane strain is treated, considering plane stress assumptions and the bending strain, in accordance with Kirchoff thin plate theory assumptions, Cheung [18]. Due to these assumptions, each strip has 8 degrees of freedom (*i.e.* 4 degrees of freedom per nodal line).

The matrix formulation is first computed with the displacement field in x, y and z local direction, corresponding to the displacements u, v and w, respectively. In order to determine the displacement in any region of the strip, the nodal displacements are interpolated with polynomials functions in the transversal direction of the strip and summations of trigonometric functions in the longitudinal direction of the strip.

First, in matrix form, the displacement field inside de strip can be approximated by Eq. (1), using the nodal line displacements $\{d\}$, and the shape function matrix $[N]$. The displacements field for each strip, $\{u\ v\ w\}^T$, is determined as a summation of all longitudinal terms, from 1 to $m \in \mathbf{N}$.

$$\begin{Bmatrix} u \\ v \\ w \end{Bmatrix} = [N]\{d\} = \sum_{p=1}^{m} \begin{bmatrix} [N_{uv}]_p & [0]_{2x4} \\ [0]_{1x4} & [N_w]_p \end{bmatrix} \begin{Bmatrix} u_1 \\ v_1 \\ u_2 \\ v_2 \\ w_1 \\ \theta_1 \\ w_2 \\ \theta_2 \end{Bmatrix}_p \qquad (1)$$

where $[N_{uv}]$ is the shape function matrix due to displacements for the membrane case and $[N_w]$ is the shape function matrix due to displacements for the bending case, given in Lazzari [25].

Defining the principle of minimum total energy in Eq. (2), the matrix formulation can be inferred. According to Cheung [18], the principle states that "*of all compatible displacements satisfying given boundary conditions, those which satisfy the equilibrium conditions make the total potential energy assume a stationary value*".

$$\left\{\frac{\partial \Pi}{\partial \{d\}}\right\} = \{0\}, \qquad where\ \Pi = U + W. \tag{2}$$

in which Π is the total potential energy, U is the elastic strain energy (Eq. (3)) stored in the body, W is the potential energy of external forces (Eq. (4)) and $\{d\}$ is the nodal displacements for all degrees of freedom and all terms of the series.

By definition, the strain energy of a three dimensional solid is defined by Eq. (3). Where $\{\varepsilon\}$ is the strain, compound by the sum of the bending and twisting curvature strain ($\{\varepsilon_B\}$) with the normal and shear strain ($\{\varepsilon_M\}$). Also, $\{\sigma\}$ is the stress, related to the strains, dV is the differential of volume, $[B]$ is the matrix with the appropriate partial differentiations of the strain-displacement relationship known as the strain matrix and $[D]$ is the elasticity property matrix.

$$U = \frac{1}{2}\iiint_V \{\varepsilon\}^T\{\sigma\}\, dV = \frac{1}{2}\iiint_V \{d\}^T[B]^T[D][B]\{d\}\, dV. \tag{3}$$

By definition, the potential energy of the external forces is defined by Eq. (4). Where $\{q\}$ is the vector with the external surface loading and dA is the differential of area.

$$W = -\iint_A \begin{Bmatrix} u \\ v \\ w \end{Bmatrix}^T \{q\}\, dA = -\iint_A \{d\}^T[N]^T\{q\}\, dA. \tag{4}$$

Introducing Eq. (3) and Eq. (4) into Eq. (2) and differentiating with respect to $\{d\}$, it leads to an equation that can be written as $[k]\{d\} - \{F\} = \{0\}$, where $[k]$ is the elastic stiffness matrix and $\{F\}$ the vector with the superficial forces applied into the plane xy of the strip.

Expanding the elastic stiffness matrix for all the terms of the series from 1 to m, and putting in a summation form and applying its limits of integration defined by the strip volume, the general elastic stiffness matrix is given by Eq. (5).

$$[k] = \sum_{k=1}^{s}\sum_{p=1}^{m}\sum_{q=1}^{m}\int_0^t\int_0^a\int_0^b [B^i]_p^T[D][B^j]_q\, dx\, dy\, dz. \tag{5}$$

The Eq. (5) shows in a compact form the elastic stiffness matrix for the finite strip method for a lower order strip with two nodal lines.

Assuming the case of plane stress (*i.e.* there are displacements only in the plane xy), it leads to the elastic stiffness matrix for the membrane, $[k_M]$. On the other hand, assuming only bending, twisting moments, and shearing forces (*i.e.* including only bending and twisting curvatures), it leads to the elastic stiffness matrix for the bending case, $[k_B]$. Both local matrices are given in Lazzari [25], to the p^{th} and q^{th} half-wave, from node i to node j (k^{th} strip).

Note that for the assumed flat shell strip (LO2), there is no interaction between the bending and the membrane cases. Due to that, the local elastic stiffness matrix is obtained by assembling the membrane and bending matrices through a simple combination, as described in Eq. (6).

$$[k^{ij}]_{pq} = \begin{bmatrix} [k_M^{ij}]_{pq} & [0]_{4\,x\,4} \\ [0]_{4\,x\,4} & [k_B^{ij}]_{pq} \end{bmatrix}_{8\,x\,8}. \tag{6}$$

For the stability problem, it is necessary to formulate the geometric matrix due to the initial stress. Whereas the finite strip element is a LO2 flat shell subjected to initial stresses that vary linearly, the distribution of the edge stress along the longitudinal axis is constant. Thus, the potential energy due to the in-plane forces is given by Eq. (7):

$$V = \frac{1}{2}\iiint_V \{\sigma_1 - (\sigma_1 - \sigma_2)\bar{x}\}\left\{\left(\frac{\partial u}{\partial y}\right)^2 + \left(\frac{\partial v}{\partial y}\right)^2 + \left(\frac{\partial w}{\partial y}\right)^2\right\} dV \tag{7}$$

Considering a uniform thickness of the strip, the edge stresses can turn into edge tractions, $T_1 = \sigma_1 t$ and $T_2 = \sigma_2 t$. Then, setting the appropriate limits of integration and computing the quadratic derivative terms into a matrix form in accordance with the nodal line displacements, the potential energy due to the in-plane forces can be deducted to a compact form. Therefore, it leads to the general expression for the geometric stiffness matrix or the initial stress matrix, given in Eq. (8).

$$[kg] = \sum_{k=1}^{s}\sum_{p=1}^{m}\sum_{q=1}^{m}\int_0^a\int_0^b \{T_1^i - (T_1^i - T_2^j)\bar{x}\}\,[G^i]_p^T\,[G^j]_q\, dx\, dy \tag{8}$$

Similar to the elastic stiffness matrix, the initial stress matrix is divided into membrane and bending cases. Solving the Eq. (8) for the membrane case, which considers the matrix with the partial derivatives of the shape functions for the plane stress, leads to the geometric stiffness matrix for the membrane. Likewise, solving the Eq. (8) for the bending case, which considers the matrix with the partial derivatives of the shape functions for the bending and twisting, leads to geometric stiffness matrix for the bending. Both local geometric matrices are given in Lazzari [25], to the p^{th} and q^{th} half-wave, from node i to node j (k^{th} strip).

Note that for the assumed flat shell strip (LO2), there is no interaction between the bending and the membrane cases. Due to that, the local geometric stiffness matrix is obtained by assembling the membrane and bending matrices through a simple combination, as described in Eq. (9).

$$[kg^{ij}]_{pq} = \begin{bmatrix} [kg_M^{ij}]_{pq} & [0]_{4\,x\,4} \\ [0]_{4\,x\,4} & [kg_B^{ij}]_{pq} \end{bmatrix}_{8\,x\,8}. \quad (9)$$

Thus, the global matrices are obtained by assembling all the half-wave terms in each corresponding degree of freedom. For the assembling, it is necessary to transform the local coordinate into global coordinates. Note that the space transformation from local to global is performed by multiplying the local matrices by a rotation matrix, $[R]$. In Eq. (10) and Eq. (11) the space transformation and global matrices assembling are defined, for the elastic stiffness matrix and geometric stiffness matrix, respectively.

$$[K] = \sum_{k=1}^{s}\sum_{p=1}^{m}\sum_{q=1}^{m}[R]_{8x8}[k^{ij}]_{pq}[R]_{8x8}^{T}. \quad (10)$$

$$[KG] = \sum_{k=1}^{s}\sum_{p=1}^{m}\sum_{q=1}^{m}[R]_{8x8}[kg^{ij}]_{pq}[R]_{8x8}^{T}. \quad (11)$$

After the assembling and space transformation, the general stability solution is obtained by solving the classic generalized eigenvalue problem described in the Eq. (12).

$$([K] - [\Lambda][KG])[\Phi] = [0] \quad or \quad [K][\Phi] = [\Lambda][KG][\Phi] \quad (12)$$

where $[K]$ is the assembled global elastic stiffness matrix (Eq. (10)), $[KG]$ is the assembled global geometric stiffness matrix (Eq. (11)), $[\Lambda]$ is the eigenvalue matrix and $[\Phi]$ is the eigenvector matrix. In other words, the matrix $[\Lambda]$ corresponds to a diagonal matrix with critical stresses and $[\Phi]$ refers to a matrix with buckling modes, where each column of the matrix represents one mode, and the first column correspond to the critical buckling mode.

Based on the present formulation, a finite strip computational program was developed, as will be presented in session 5.

3. Distortional-Global Couple Instability Phenomenon concepts

The DG buckling interaction can be classified into its type and nature. As reported by Martins *et al.* [14], the type of distortional-global interaction can change depending on the form of the global buckling mode: (*i*) distortional/major-axis flexural-torsional (D-FT) and (*ii*) distortional/minor-axis flexural (D-F). However, for lipped channel columns, the D-FT interaction is more common to occur, while the D-F interaction happens more often on zed-sections columns. In addition, related to the nature of the critical buckling load, Martins *et al.* [14] states additional classification. This categorization is based on the ratio between the critical loads from global and distortional modes, $R_{GD} = P_{crG}/P_{crD}$, and it is useful for performing a parametric structural behavior study. The categories are classified as:

(i) True DG interaction (TI): When the distortional and global critical buckling are close, this scenario may always happen for $0.90 < R_{GD} < 1.10$. According to Martins *et al.* [14], this state can behave differently in three different groups, depending on the critical slenderness: (*i*.1) abruptly collapse for stocky columns, $\lambda_{cr} \leq 1.0$; (*i*.2) collapse after starting of yielding for slender columns, $1.0 < \lambda_{cr} < 2.0$; (*i*.3) elastic-plastic strength reserve before collapse for very slender columns, $\lambda_{cr} \geq 2.0$ (this group has shown local deformations, experiencing LDG interaction on lipped channel columns).

(ii) Secondary-distortional bifurcation DG interaction (SDI): Occurs for yield strength sufficiently high, in order to enable the interaction to develop. This situation is more common in the range $R_{GD} \leq 0.90$.

(iii) Secondary-global bifurcation DG interaction (SGI): Also occurs for yield stress sufficiently high, to enable the interaction to arise, nonetheless this one is more likely to develop, due to its high post-critical strength reserve caused by the distortional buckling. This is more common in the range $R_{GD} \geq 1.10$.

4. Design Procedures for DG buckling Interaction

In general, the design procedures for CFS columns are based on a previously elastic buckling analysis, in order to determine the critical buckling load, which is a crucial parameter to estimate the strength capacity of the CFS columns. The direct strength method (DSM) is the most known design procedure for CFS members. The method has a simple application for civil engineers' design of thin-walled structural elements, based on the limit states associated with local, distortional, global and the local-global interactive modes. The DSM is based on the Winter-type equation [26] & [27] for the local and distortional curves, and the "classical" design curve for the global mode, taken from specifications of hot-rolled steel structures (*e.g.* ABNT NBR 8800:2008 [28] and ANSI/AISC 360-16 [29]).

The DSM equations are described for columns. One advantage of the DSM procedure is the capacity to expresses straightforward interactive equations, as shown

by Schafer [30]. In the past few years, additional equations have been proposed considering interactive modes and also recalibration of the Winter-type equation [26] coefficients.

The nominal axial strength for the global buckling, P_{nG}, is obtained as described in the DSM. The Eq. (11) expresses the nominal strength due to global buckling.

$$P_{nG} = \begin{cases} P_y\, 0.658^{{\lambda_G}^2}, & \lambda_G \leq 1.5 \\ P_y \dfrac{0.877}{{\lambda_G}^2}, & \lambda_G > 1.5 \end{cases} \qquad \lambda_G = \sqrt{\frac{P_y}{P_{crG}}} \quad (11)$$

where P_y is the squash load, defined as the gross cross-sectional area times the steel yielding stress; λ_G is the global slenderness; and P_{crG} is the elastic critical global buckling load.

The nominal axial strength for the distortional buckling, P_{nD}, is obtained as described in the DSM by Eq. (12)

$$P_{nD} = \begin{cases} P_y, & \lambda_D \leq 0.561 \\ \dfrac{P_y}{{\lambda_D}^{1.2}}\left(1 - \dfrac{0.25}{{\lambda_D}^{1.2}}\right), & \lambda_D > 0.561 \end{cases} \qquad \lambda_D = \sqrt{\frac{P_y}{P_{crD}}} \quad (12)$$

where P_y is the squash load, defined as the gross section area times the steel yielding stress; λ_D is the distortional slenderness; P_{crD} is the elastic critical distortional buckling load.

The nominal axial strength for the distortional-global (DG) interactive buckling has not been included yet in the standards. In the past few years, authors have been studying the distortional-global coupled phenomenon behavior, in Dinis and Camotim [13] and Martins *et al.* [31]. However, there is still a lack of studies of this phenomenon, mainly lacking laboratory experiments. Nevertheless, Schafer [30] proposed an approach to the DSM that consider the distortional-global interaction, P_{nDG}, shown in Eq. (13). In addition, the recent study carried out by Martins *et al.* [14], uses the procedure proposed by Schafer [30] with a parametric study, with results showing that the procedure is quite conservative, comparing with the global equation approach in Eq. (11). Martins *et al.* [14] also studied an additional approach that includes the distortional-global interaction, P_{nGD}, shown in Eq. (14).

Basically, the approach in Eq. (13) involves in replacing the squash load P_y from the distortional buckling equation (Eq. (12)) by the nominal strength for global buckling P_{nG} (Eq. (11)). Likewise, in Eq. (14), the approach consists of replacing the squash load P_y from the global buckling equation (Eq. (11)) by the nominal strength for the distortional buckling P_{nD} (Eq. (12)).

$$P_{nDG} = \begin{cases} P_{nG}, & \lambda_{DG} \leq 0.561 \\ \dfrac{P_{nG}}{{\lambda_{DG}}^{1.2}}\left(1 - \dfrac{0.25}{{\lambda_{DG}}^{1.2}}\right), & \lambda_{DG} > 0.561 \end{cases} \qquad \lambda_{DG} = \sqrt{\frac{P_{nG}}{P_{crD}}} \quad (13)$$

$$P_{nGD} = \begin{cases} P_{nD}\, 0.658^{{\lambda_{GD}}^2}, & \lambda_{GD} \leq 1.5 \\ P_{nD} \dfrac{0.877}{{\lambda_{GD}}^2}, & \lambda_{GD} > 1.5 \end{cases} \qquad \lambda_{GD} = \sqrt{\frac{P_{nD}}{P_{crG}}}. \quad (14)$$

5. FStr Computer Application

In order to perform elastic buckling analysis of CFS members, a finite strip method-based solution was implemented. This computational tool made easier for the authors to perform the buckling analysis.

FStr Computer Application is a software with graphical user interface (GUI) developed on the basis of the Finite Strip Method (FSM) formulation. The FStr is implemented in MATLAB platform (MathWorks [32]) and is inspired in the CUFSM 5 [33] and GBTul 2.0 [34] graphical user interface. The program folder presentation is illustrated in Figure 1 (the graphical user interface application itself is not an open source software, however, it is free for use).

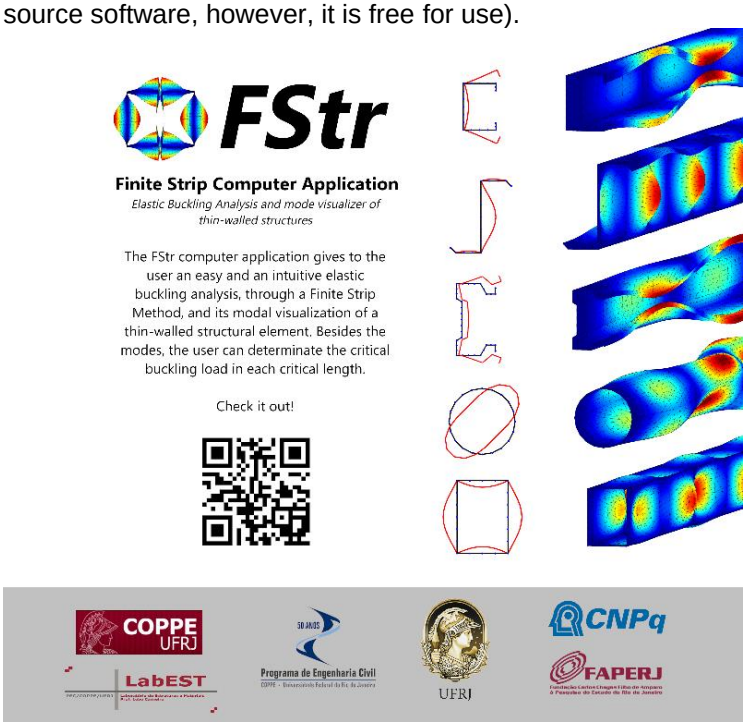

Figure 1: Finite Strip Computer Application presentation folder. https://sites.google.com/coc.ufrj.br/fstr/

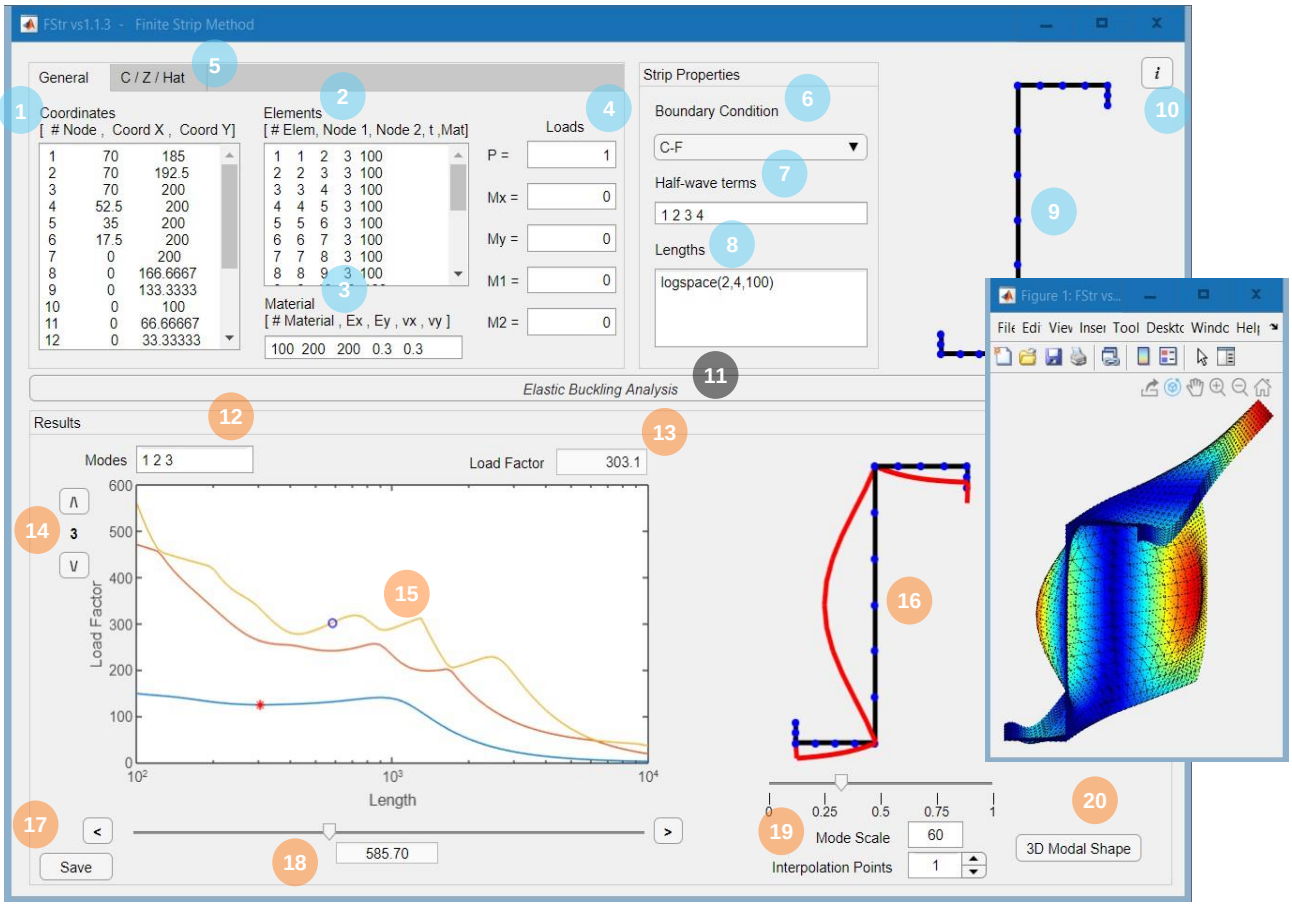

Figure 2: Finite Strip Computer Application Graphical User Interface index description.
<https://sites.google.com/coc.ufrj.br/fstr/>

The purpose of the GUI is to make it easier to the user to set up the data input and to analyze the data output. Figure 2 shows the FStr GUI with the data input and output displayed in a single window.

(1) Coordinates Panel;
(2) Elements Panel;
(3) Orthotropic Material Panel;
(4) Loading (axial compression and/or pure bending);
(5) Automatic cross-section generation;
(6) End Boundary Condition(S-S, C-S, C-F, C-G, C-C);
(7) Half-wave terms for trigonometric series;
(8) Set of lengths of structural element;
(9) Dynamic 2D cross-section geometry;
(10) About the FStr Computer Application;
(11) Elastic Buckling Analysis Button;
(12) Number of superior modes displayed;
(13) Critical Load/Moment Factor;
(14) Selection of Superior Modes;
(15) Load Factor *vs* Length (signature curve for p=1);
(16) Dynamic 2D Modal Shape, for each Length and Transversal Position Ratio ($\bar{y} = y/L$);
(17) Save in *.txt* or *.mat* format;
(18) Selection of Length;
(19) Mode Scale and Interpolation points changer;
(20) 3D Modal Shape for the selected Length.

The FStr was validated in Lazzari [25] with the help of 9 different models in 4 types of validation. First, 5 models of flat rectangular plates under compression were analyzed, with 5 different boundary condition (S-S, C-S, C-F, C-G and C-C) on the extremities and free in the longitudinal edges. Secondly, 5 more flat rectangular plates with longitudinal clamped edges under compression were analyzed. Thirdly, a more complex model of a lipped channel column was analyzed, with simply-simply and clamped-clamped end condition. Lastly, a stiffened lipped channel and a zed section beam were analyzed, under uniform unrestricted bending and simply-simply supported end condition.

The FStr is a free computer application program, able to perform elastic buckling analysis for research activities and engineering design of thin-walled structures. The program can be accessed in the website

<https://sites.google.com/coc.ufrj.br/fstr/>, or GitHub website <https://github.com/joaoadelazzari/FStr>, or in the file exchange from MathWorks website <https://www.mathworks.com/matlabcentral/fileexchange/74306>.

6. Finite Element Method Model

The FEM numerical model performs an important task for the parametric study of CFS columns under DG buckling interaction. Through a calibrated finite element model, based on experimental tests, the model can reproduce real experiments numerically. This approach saves time in order to perform a parametric study, and also leads it to a more practical structural investigation that is almost impossible to test in real physical conditions.

Figure 3 shows an illustration of a CFS column with a lipped channel section and both ends fixed. This figure illustrates some of the main components of the numerical model, as discretization, end boundary condition and loading. In Figure 3-a is illustrated the meshes, as well as the actual thickness of the end plate and the structural CFS element. Figure 3-b and Figure 3-e display both end boundary condition with the loading and restrictions. Figure 3-c also exhibits the mesh, but in the structural element. Finally, Figure 3-d shows the restriction on longitudinal direction.

6.1. Discretization

The type of element is restricted to a shell type, SHEEL281 (ANSYS Theory Reference [35]), which has 8 nodes, with 6 degrees of freedom. This type of element is adequate for analyzing thin to moderately-thick shell based structures and it is appropriate for linear, large rotation and large strain nonlinear situations. Secondly, the mesh properties include a mixed mesh with quadrilateral and triangular shell element with a fixed element size of 5 by 5 mm (see Figure 3-a and Figure 3-c). The mesh dimensions were decided after series of convergence tests, showing that this is an appropriate solution for the present study. É ISSO?

6.2. End boundary conditions

With respect to the boundary conditions, the column has fixed-fixed end condition. The constraints in the extremities of the column are designed to be a stiff plate rigidly fixed to the end of the column, following the experimental conditions reported in the literature. Both extremities of the column

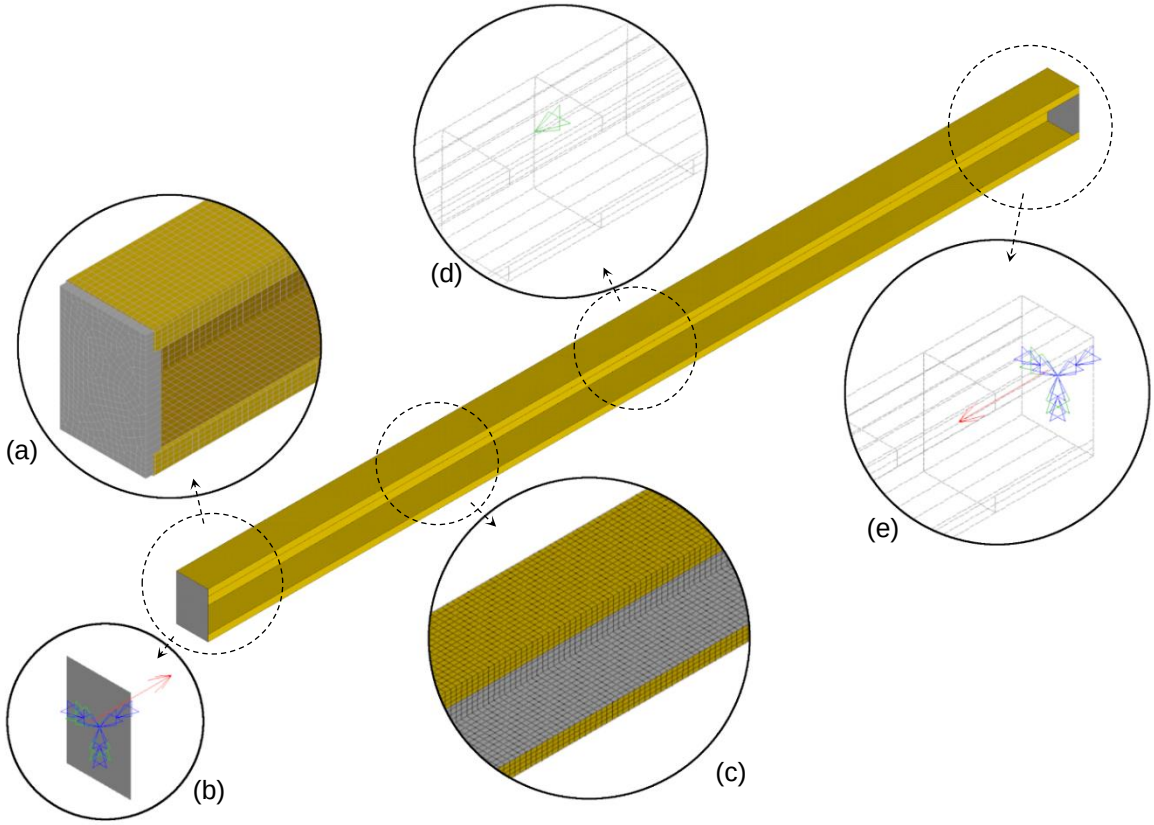

Figure 3: Finite Element Model description: (a) Shell element mesh and thickness on fixed-ended end; (b) boundary condition and axial compression loading; (c) mesh of structural element along the length; (d) dof restriction, related to the longitudinal direction at mid span; (e) boundary condition and axial compression loading at the end section.

have constraints on displacements in *x* and *y* direction, and constraints on rotation in *x*, *y* and *z* direction (see Figure 3-b and Figure 3-e). Additional z direction constraint was included at the mid span of the column preventing free body displacement (see Figure 3-d). The end plates thickness is 12 mm, based on laboratory experiments performed by Salles [36] and Santos [37].

6.3. Loading

Since the numerical model is a column, the only type of loading are the concentrated axial compressive forces (see Figure 3-b and Figure 3-e).

6.4. Material Model

The material model is defined as a balance of simplicity and accordance with reality, in order to perform acceptable parametric study. In this case, a material with bilinear isotropic hardening (elastic-perfect plastic model) is considered, which applies the von Mises yield criteria with an isotropic work hardening presumption. This hardening assumption consider an initial slope of the strain-stress curve with an elastic modulus in the elastic strain region and a tangent slope modulus (E_t) with zero magnitude in the plastic strain region. The yield strength of the material varies, depending of the column example. On the other hand, the Young modulus is 200 GPa (200 kN/mm^2) and the major Poisson's ratio equal 0.3 for all the columns. The same material properties were considered for the plates rigidly fixed at the ends of the columns.

With respect to the residual stresses and cold bending corner effects, the major part of investigations neglected these effects. Dinis and Camotim [38] reported insignificant impact in the ultimate column load related to the variation of these effects. Also, according to Ellobody and Young [39], the small membrane residual stresses has been demonstrated an irrelevant effect on the ultimate load, stiffness of the column, load-shortening behavior and in the failure mode. In Matsubara *et al.* [12], a recent finite element modeling of local-distortional coupled phenomena in lipped channel CFS columns, the residual stresses and rounded corners effects were also neglected and accurate comparison between numerical and experimental results was found.

6.5. Initial geometric imperfections

For the present work the original perfect geometry and imperfections of the column are created with the help of a previous FSM analysis. The FStr program (described in section 5) performs the elastic buckling analysis and, with the buckling modal critical shape, generates coordinates that are inserted into an APDL (Ansys Parametric Design Language) routine code. The modal critical shape is inserted as an initial geometric imperfection, with a maximum amplitude depending on the mode.

The maximum amplitudes parameters for global and distortional buckling are different. As initially proposed by Martins *et al.* [14], the present research adopts $L/1000$ for global imperfection and $0.94t$ for distortional imperfection. The reason for the distortional imperfection value is presented by Schafer and Pekoz [40], as corresponding to 50% probability that a random imperfection amplitude is below or above this value. However, in the study of Santos [41], with end-bolted CFS columns under distortional critical length, it has been shown that the ultimate load has not changed excessively with the variation of the maximum amplitude from $0.1t$ up to $1.0t$ (failure load variation below 5%). Anyway, $0.94t$ is adopted and applied to the distortional buckling initial geometric imperfection amplitude.

6.6. Analysis Methods

For the present case material and geometry nonlinearities are considered in a post-buckling behavior. The ANSYS built-in method to execute this type of analysis is based on the arc-length method, known as "*The modified Riks method*" (introduced by Riks [42], [43] and Wempner [44]). The method assumes displacement control strategy during the loading, in order to find the fundamental paths before and after the limit load. This method is convenient for solutions of unstable problems displaying a nonlinear static equilibrium.

6.7. Numerical model validation

Since there is an absence of laboratory testing experiencing the DG interaction in lipped channel columns, the finite element model is validated for columns that demonstrated only global buckling mode and distortional buckling mode, before collapsing.

For the global buckling mode validation, the experimental results from Heva [45] are taken. The validation consists of the comparison of the equilibrium paths and ultimate load from Heva [45] with the presented numerical model. Heva's [45] specimens consisted of three columns with same length (experiencing global elastic buckling mode), but different geometry and material properties. The validation is performed using a bilinear and multilinear isotropic hardening material model. The complete validation analysis is provided in Lazzari [25].

For the distortional buckling mode validation, the experimental results from Salles [36] are taken. The validation consists of the comparison of the equilibrium paths and ultimate load from Salles [36] with the presented

numerical model (Figure 3). Salles' [36] specimen consisted of one column in a length experiencing 3 half-waves of distortional elastic buckling mode. The complete validation analysis is also provided in Lazzari [25].

The obtained results of the validation in Lazzari [25] allow concluding that the developed finite element model is validated for flexural-torsional and distortional post-buckling analysis.

7. Parametric analysis on DG buckling coupled phenomenon

The numerical study is addressed to a set of lipped channel cold-formed steel columns under true DG interaction, with different combinations of initial geometric imperfections. Additionally, the study included variation of the yield stress and longitudinal length in order to observe and understand the column structural behavior of DG interaction in a large range of slenderness.

The parametric analyses performed in the present research consist of cold-formed lipped channel columns with section out-to-out dimensions: b_w = 100 mm, b_f = 70 mm, b_l = 15 mm, t = 2.70 mm (LC 100x70x15x2.70, see detail in Figure 4). The variable parameters are: initial geometric imperfection, column length and yield stress.

7.1. Study of Initial Geometric Imperfection Combination

This study consists in analyzing the structural behavior of the cold-formed lipped channel section LC 100x70x15x2.70 mm (out-to-out dimensions) with L=1850 mm with different initial geometric imperfections and steel yield strength. The goal of this study is to identify the column's strength and behavior sensibility related to the initial geometrical imperfections, using "impure" modal combination, in opposition of only taking the fundamental D and G pure buckling modes. The geometry is determined for a column experiencing strong DG buckling interaction, for a length L characterizing True DG interaction (TI).

The modal combination is performed using the first and the second mode shape, for a length of 1850mm. The first mode is a Global (flexural-torsional) elastic buckling mode (G), with 88.6% of pure global buckling mode (given by CUFSM [33] modal participation in vector norm) and critical buckling load of 354.5 kN. On the other hand, the second mode is a

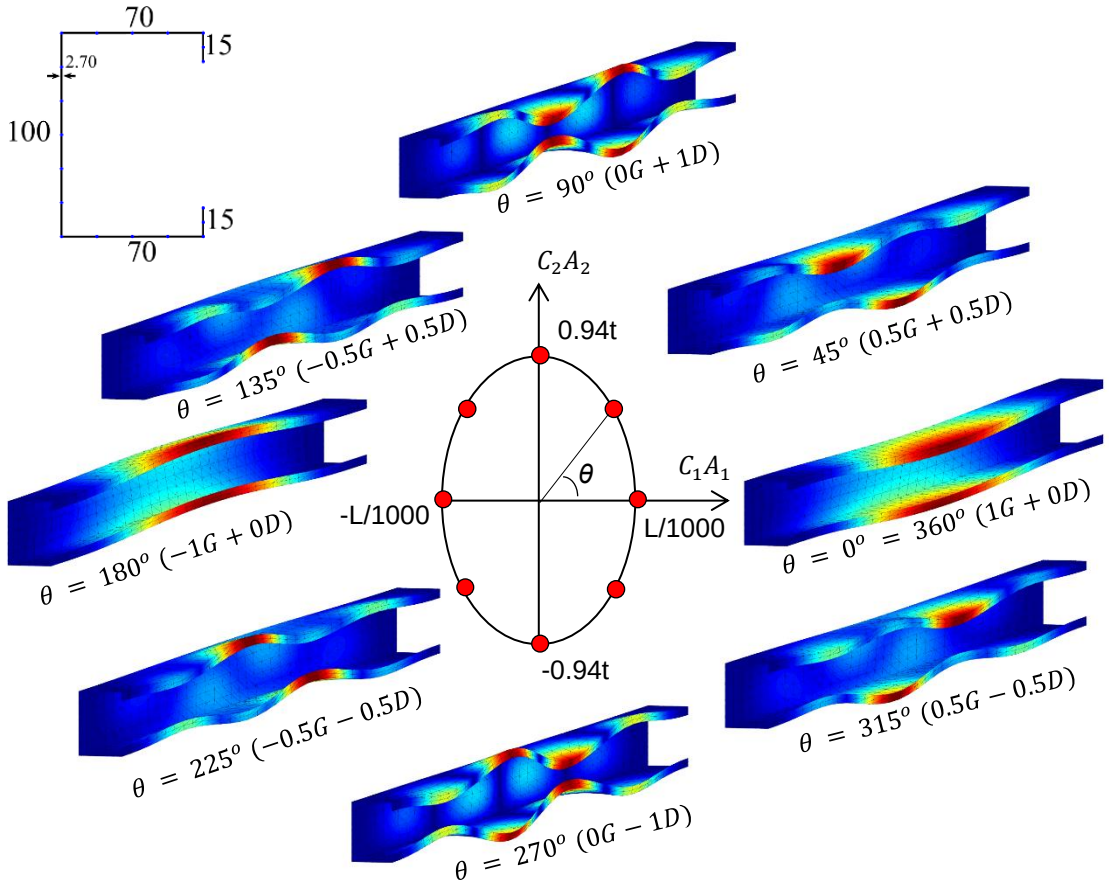

Figure 4: Analogy of modal shape initial imperfection combination in function of $\boldsymbol{\theta}$, initial imperfection parameter (modal shapes amplified 10 times).

distortional elastic buckling (D), with 95.8% of pure distortional buckling mode with 4 half-waves (given by CUFSM [33] modal participation in vector norm) and critical buckling load of 356.2 kN.

In order to illustrate the modes combination, Figure 4 shows the initial imperfection combination in a "trigonometric ellipse", where: $C1 = cos(\theta)$; $C2 = sin(\theta)$; θ is an angle related to the changing of the modal combination; A_1 and A_2 are the maximum amplitude for initial geometric imperfection, for the first and second modes, respectively.

This idea of combining the buckling modes in a "trigonometric ellipse" (Figure 4) is inspired in a similar procedure proposed by Martins *et al.* [14]. Basically, the parameter θ is a single parameter that allows changing the initial geometric imperfections and consequently the modal combination shape. More information about how the initial imperfections are combined, is given in Lazzari [25].

Basically, the columns with initial geometric imperfection combination from $\theta = 0^o$ until $\theta = 180^o$ (first and second quadrant) are the same columns with $\theta = 180^o$ until $\theta = 360^o$ (third and fourth quadrant). Indeed, according to Lazzari and Batista [46], this symmetric behavior is predictable, because in theory, the initial geometric imperfections were basically rotated, *i.e.* the modes were multiplied by minus one.

Moreover, it is noticed another cyclic and symmetric behavior for the imperfection combination from first and second quadrant. To conclude this assumption, a deeper analysis based on accurate observation of the equilibrium paths of the columns is required to avoid mistaken conclusions. In this case, the post-buckling equilibrium paths for $\theta = [0^o, 180^o]$, spaced with an increment of 15^o, are illustrated below in Figure 5 and Figure 6, for the displacements NT4 and NT5, respectively. Each figure reveals the FEM results of the post-buckling paths for a different point in the cross-section.

Comparing the post-buckling paths (Figure 5 and Figure 6), a symmetric behavior between the initial imperfections with $\theta = [0^o, 90^o]$ and $\theta = [90^o, 180^o]$, is detected. Analyzing the NT4 and NT5 displacements, it is found that the initial imperfections with $\theta = [0^o, 90^o]$ for the NT4 displacement, has the same behavior as the initial imperfection with $\theta = [90^o, 180^o]$ for the NT5 displacement, as well as vice-versa. The same behavior happens when comparing the displacement in other points along the column and with higher yield stress (508 MPa, 1016 MPa and 1523 MPa), as reported in Lazzari [25]. Basically, this symmetric behavior evidences a "mirroring" behavior of the initial imperfection with θ from the first and second quadrant. This conclusion supports the parametric analysis of a large set of columns, to be conducted only with the initial imperfection for $\theta = [0^o, 90^o]$.

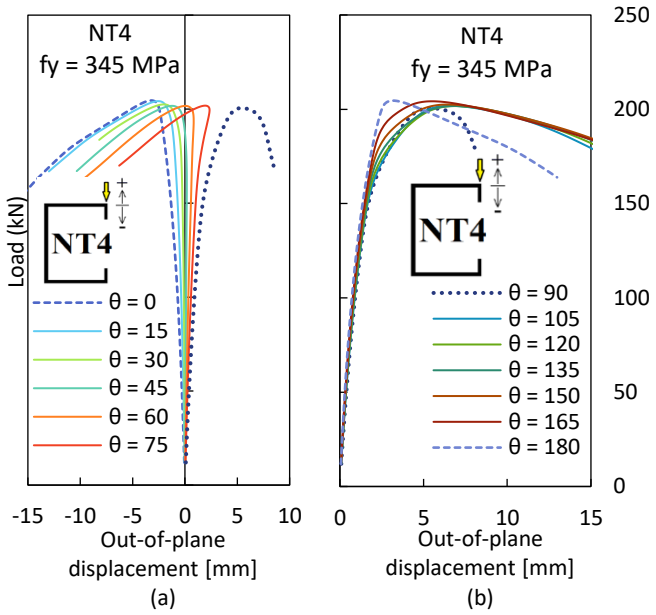

Figure 5: Post-buckling equilibrium paths, load steps vs. out-of-plane displacement NT4, with $f_y = 345\ MPa$ and $P_{cr} = 354.5\ kN$ ($P_y/P_{cr} = 0.7$) at $0.4L$, from (a) $\theta = [0^o, 90^o]$ and from (b) $\theta = [90^o, 180^o]$.

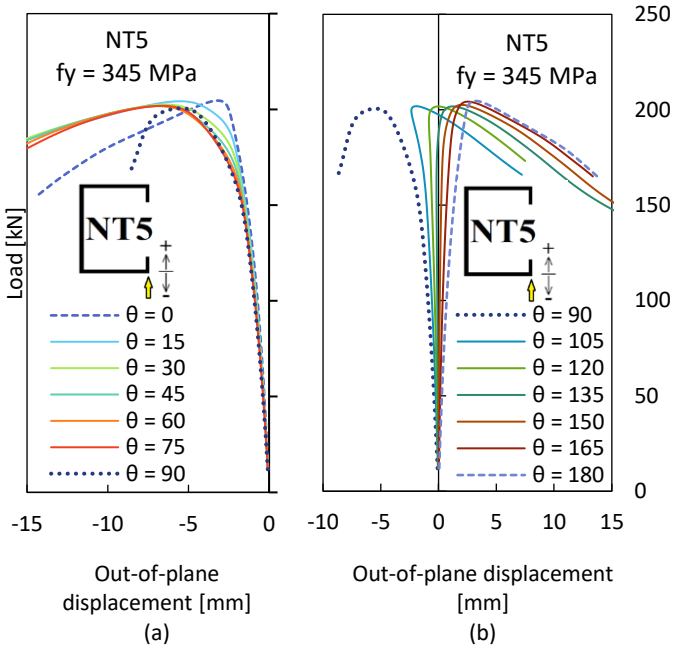

Figure 6: Post-buckling equilibrium paths, load steps vs. out-of-plane displacement NT5, with $f_y = 345\ MPa$ and $P_{cr} = 354.5\ kN$ ($P_y/P_{cr} = 0.7$) at $0.4L$, from (a) $\theta = [0^o, 90^o]$ and from (b) $\theta = [90^o, 180^o]$.

7.2. Imperfection Combination with different yield stress

The next step is to investigate columns with higher yield strength. The same analysis conducted for columns with 345 MPa ($P_y/P_{cr} = 0.7$) yield stress, are performed for

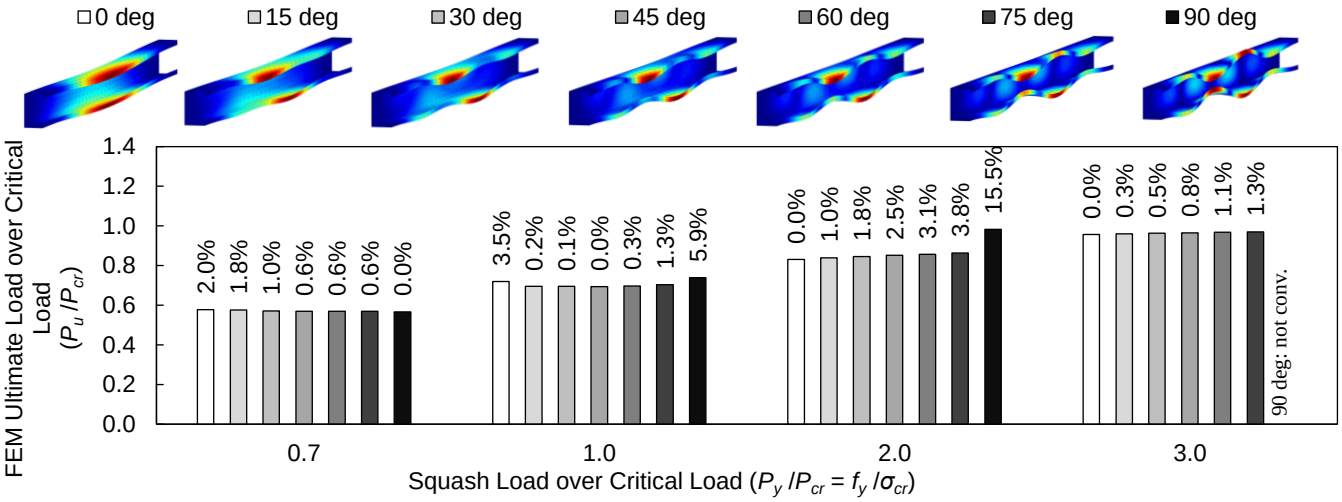

Figure 7: P_u/P_{cr} vs. P_y/P_{cr} of columns under different IGI combination, $\theta = [0^o, 90^o]$ and with yield strength of 345 MPa, 508 MPa, 1016 MPa, and 1523 MPa.

columns with 508 MPa ($P_y/P_{cr} = 1.0$), 1016 MPa ($P_y/P_{cr} = 2.0$), 1523 MPa ($P_y/P_{cr} = 3.0$) and an elastic behavior analysis ($P_y/P_{cr} \rightarrow \infty$), taking $\theta = [0^o, 90^o]$ ‡.

Comparing the strength of these columns with different initial geometric imperfection combination and different yield strength, it is possible to notice which initial imperfection has more influence in the column's load capacity. Figure 7 shows the column strength P_u *vs.* squash load P_y, normalized with critical load in both axes. As it was expected, for more slender columns, the ultimate load increases. For $P_y/P_{cr} = 0.7$, the lower ultimate load occurs with only distortional initial imperfection ($\theta = 90^o$). However, for $P_y/P_{cr} = 1.0$, the most detrimental strength takes place with 50% of global and 50% of distortional mode contribution ($\theta = 45^o$ or 0.5G+0.5D) of initial imperfection. Moreover, for high yield stress, the lower ultimate load is affected with only by global initial imperfection ($\theta = 0^o$).

Basically, the proposed study of initial geometric imperfection combination allowed a deep understanding of the complex behavior of the True DG buckling interaction (TI). It has shown that the different initial imperfection combination affects the ultimate load and structural behavior for a column under the TI DG buckling interaction nature. The following study consists of evaluating the performance of the load capacity of columns in Secondary-distortional bifurcation DG interaction (SDI) and Secondary-global bifurcation DG interaction (SGI) regions.

7.3. Study of DG buckling interaction nature

This study consists in investigating columns with different slenderness factors, in order to understand the influence of the interaction nature in the column strength. For this study the section LC 100x70x15x2.70 mm is considered, the same geometry employed in the initial geometric imperfection combination analysis. However, the length of the column is modified. This changing of column's length permits the variation of the global and distortional slenderness ratios and its contribution on the column behavior.

Basically, the investigation is performed for columns with the three different natures: SGI, TI and SDI. In the sense of illustrating graphically the DG interaction nature investigation, Figure 8 shows the results of FStr computation for the critical load versus $R_{\lambda GD}$ curve in contrast with the pure local, distortional and global buckling mode curves (where $R_{\lambda GD} = \lambda_G/\lambda_D = \sqrt{P_{crD}/P_{crG}}$). The slenderness ratio $R_{\lambda GD}$ measures how far the critical loads of global and distortional modes are from each other. According to Martins *et al.* [14], when $0.95 < R_{\lambda GD} < 1.05$ there is TI, $R_{\lambda GD} \geq 1.05$ there is SDI and $R_{\lambda GD} \leq 0.95$ there is SGI (where $R_{\lambda GD} = \sqrt{1/R_{GD}}$, since this author employs $R_{GD} = P_{crG} / P_{crD}$ as the main factor for the evaluation of DG buckling interaction).

Notice in Figure 8 that $R_{\lambda GD} = 0.84$ represents the length of 1500 mm, $R_{\lambda GD} = 1.10$ is correlated with length of 1850 mm and $R_{\lambda GD} = 1.18$ is associated with length of 2200 mm. As can be observed, the range of SGI and SDI is not that extensive, because the analysis is limited to only one cross-section geometry. For a deeper understanding of the DG buckling interaction nature, it would be necessary a wider variety of cross-section geometries (larger $R_{\lambda GD}$ range). The analysis performed in this research is focused on the TI nature, with fewer columns in the SGI and SDI regions.

‡ The results for these analysis are shown in Appendix B of the master's thesis of Lazzari [25].

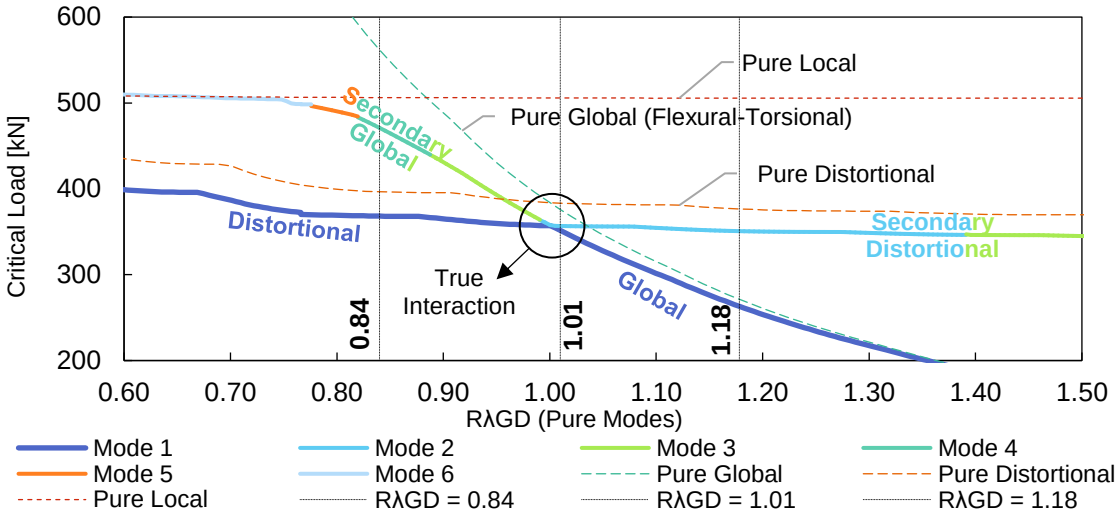

Figure 8: Critical load vs. $R_{\lambda GD}$ for LC 100x70x15x2.70 mm, illustrating SGI, TI and SDI regions in all mode analysis and pure mode analysis.

As a result of the initial geometric imperfection combination analysis, the following parametric study consists of using two different initial geometric imperfection (1G+0D and 0.5G+0.5D, *i.e.* $\theta = 0^o$ and $\theta = 45^o$, respectively) for three different yielding stresses, 345 MPa, 508 MPa and 1016 MPa, *i.e.* applying 1G+0D with the three yield stress, and 0.5G+0.5D with the same three yield stresses. For each of these yield stresses, the column strength capacity is reached, for 15 lengths (from 1500 mm to 2200 mm with increment step of 50 mm), and compared with the actual global (Eq. (11)) and distortional direct strength method (Eq. (12)) equations. In addition, the column strength is compared with the proposed DG buckling interaction equations, proposed by Schafer [30] (Eq. (13)) and by Martins *et al.* [14] (Eq. (14)).

In order to compare the ultimate load with the available standard DSM approach, Figure 9 and Figure 10 provide a graphical illustration, where $P_{nDSM} = min(P_{nLG}, P_{nD}, P_{nG})$, and P_{nLG} is given by Eq. (2.64), P_{nD} by Eq. (12) and P_{nG} by Eq. (11). Figure 9 shows the results for 50% distortional + 50% global initial imperfection combination, and Figure 10 exhibit the results for 100% global initial imperfection combination.

It is noticeable in Figure 9 and Figure 10 that as larger is the elastic behavior range, corresponding to higher yielding stress, the lower is the P_u/P_{nDSM} ratio, for $R_{\lambda GD} < 1.08$ with 0.5G+0.5D initial geometric imperfection combination, and for $R_{\lambda GD} < 1.15$ with 1G+0D initial geometric imperfection combination. Additionally, these columns with lower values of $R_{\lambda GD}$ ($R_{\lambda GD} < 0.87$) and higher yielding ($f_y = 1016\, MPa$), seem to diverge from the standard DSM, due to a possible DG buckling interaction in a SGI region. Lastly, comparing the two cases of initial imperfection combination, it is noticed that the mean, maximum and minimum value of P_u/P_{nDSM} ratio, are similar to each type of imperfection, while the 0.5G+0.5D initial imperfection combination presents the lower standard deviation and coefficient of variation.

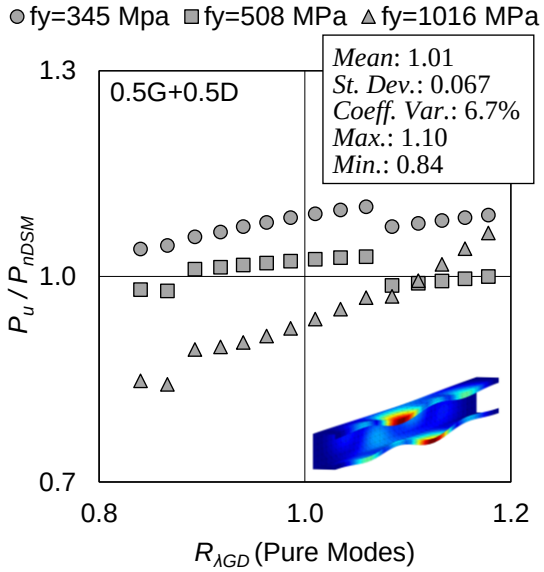

Figure 9: FEM Ultimate Load over standard DSM Nominal Axial Strength versus DG slenderness ratio, considering 50% global + 50% distortional initial imperfection.

Figure 11 shows the numerical strength results compared with the design approaches P_{nG} (Eq. (11)), P_{nD} (Eq. (12)), P_{nDG} (Eq. (13)), and P_{nGD} (Eq.(14)).

The graph in Figure 11 shows how disperse the ultimate load (P_u) are from the DSM-based equations (P_n). Notice that the P_{nD} procedure is clearly not corresponding to the column's strength. Furthermore, the P_{nG}, P_{nGD}, and P_{nDG} appears to be more stable approaches, even though the

P_{nGD} and P_{nDG} procedures have shown to be quite conservative (points along the line -5% of $P_n = P_u$).

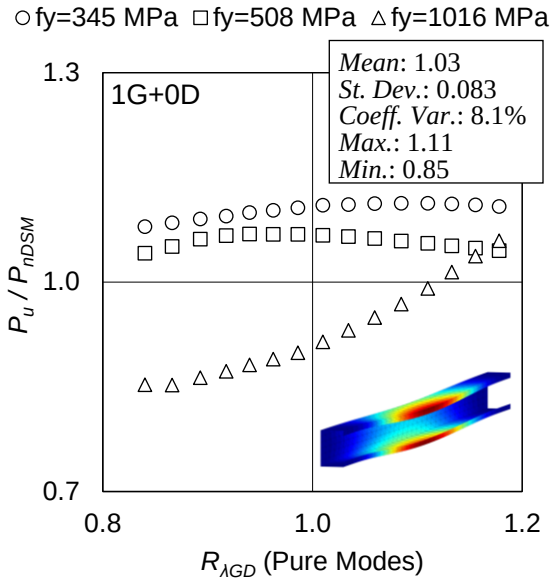

Figure 10: FEM Ultimate Load over standard DSM Nominal Axial Strength versus DG slenderness ratio, considering 100% global initial imperfection.

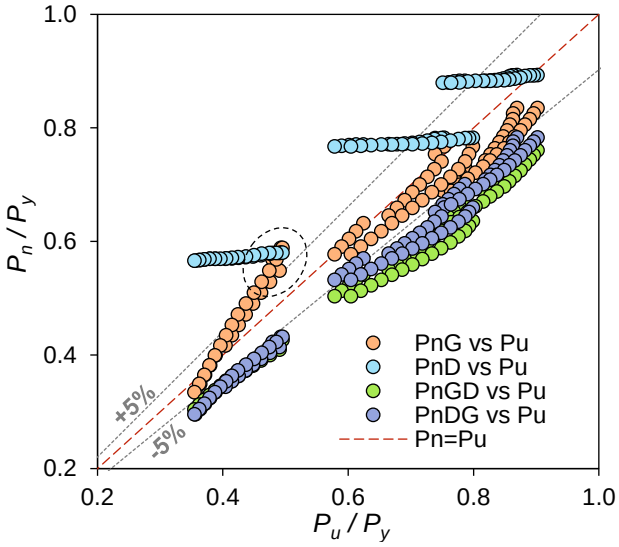

Figure 11: Numerical Column Strength over Squash Load (P_u/P_y) results, with different yield stress and Initial Geometric Imperfection, compared with the DSM-based equations (P_{nG}, P_{nD}, P_{nGD}, and P_{nDG}).

Another approach to visualize the FEM results P_u is to display the corresponding data into the traditional column strength design curve (P_u/P_y) *versus* global slenderness factor (λ_G), taking the DSM nominal column strength equation, restricted to the global buckling mode (Eq. (11)). This graphical data illustration is exposed in Figure 12. This figure basically shows all the 90 columns strength over squash load ratio *versus* the global buckling slenderness factor, in addition with the global buckling DSM equation (Eq. 11) and the Euler column curve for reference $1/\lambda_G{}^2$.

Notice in Figure 12, that the difference of the 0.5G+0.5D and 1G+0D initial geometric imperfection in the global DSM equation is negligible. One important observation is the influence of the yielding stress. For yielding of 345 and 508 MPa, the P_u/P_y ratios are above the P_{nG} equation, while for yielding of 1016 MPa, the P_u/P_y these ratios are mostly below the P_{nG} equation. These results indicate that the global buckling DSM equation handles well for the lipped channel columns under different DG types of buckling interaction nature (*i.e.* TI, SDI and SGI).

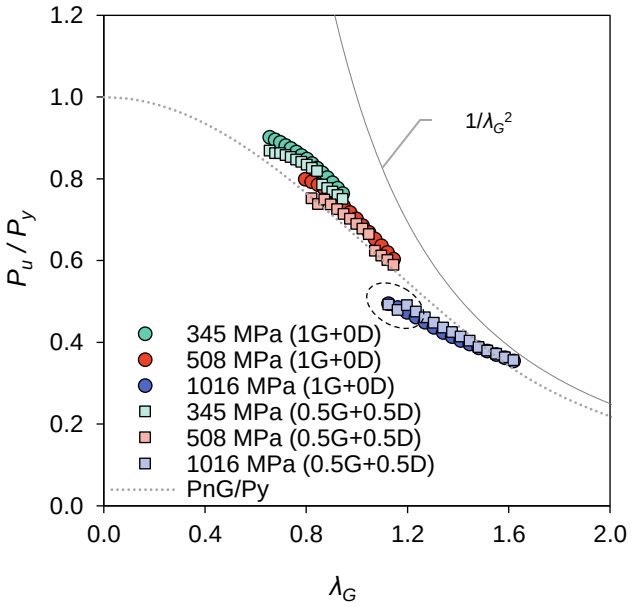

Figure 12: Numerical Column strength over Squash Load (P_u/P_y) results, with different yield stress and Initial Geometric Imperfection, compared with the global buckling DSM equation Eq. (11) and Euler $1/\lambda_G{}^2$ curve.

One important observation can be retrieved from the data inside the dashed circles in Figure 11 and Figure 12, related to the data from 1016 MPa compared with the P_{nG} equation. The data with P_u/P_y in the range of $R_{\lambda GD} < 0.87$ (*i.e.* $\lambda_G \approx 1.20$) seems to be far from the DSM nominal axial strength for global buckling (see data inside dashed circles Figure 11 and Figure 12). However, these values of nominal axial strength are close to the distortional equation (see dashed circle in Figure 11). These results are an interesting finding, indicating that these columns are probably in a region of distortional failure, or perhaps in a weak DG coupled phenomenon failure, under SGI (secondary-global bifurcation DG interaction nature).

8. Final Remarks

The present research mainly provided (i) a FSM-based elastic buckling computational analysis tool and (ii) FEM

results addressed to the improvement of the comprehension of the distortional-global interaction buckling phenomenon, including both (ii-a) its post-buckling behavior and (ii-b) the column ultimate load and strength. The investigation was addressed to CFS lipped channel columns, since these are CFS widely applied in steel construction and are prone to develop DG of buckling interaction.

The FSM computer application program, FStr, was developed in order to assist the elastic buckling analysis. The program, implemented in MATLAB, has an accessible and easy graphical user interface and was conceived to attend research activities as well as engineering design of steel thin-walled structures.

With respect to the parametric analysis on DG buckling coupled phenomenon, some interesting remarks must be pointed out. The analysis was divided in three major studies: (i) study of the effect of the initial geometric imperfection combination; (ii) study of initial imperfection combination with different yield stresses, and (iii) study of DG buckling interaction nature.

In relation to the study of initial geometric imperfection combination, the following remarks must be reported:

(i) Combining the initial geometric imperfection as first and second mode (which were classified as global and distortional buckling mode), was an approach to include the distortional-global coupled phenomenon behavior into the post-buckling analysis, which was not clearly predictable by the elastic buckling analysis;

(ii) It was noticed an additional symmetric behavior. The post-buckling equilibrium path results, with $0^o \leq \theta \leq 180^o$, show "mirroring" behavior in the ranges $0^o < \theta < 90^o$ and $90^o < \theta < 180^o$. This conclusion indicates that the next FEM analyses will be satisfactorily completed by simply varying θ from 0^o to 90^o.

Regarding the study of initial imperfection combination with different yield stress, the following comments are highlighted:

(i) For columns with higher yield stress (higher slenderness, developing larger elastic equilibrium path) and the geometric imperfections in the range $0^o \leq \theta < 90^o$, it was evident the predominance of the global mode with larger displacements. On the other hand, columns with lower yield strength (less slender columns) developed pronounced distortional buckling mode in the very beginning of the loading process, showing the distortional initial imperfection has a significant influence at the early steps of the loading;

(ii) It has been shown that columns with lower yield stress, the distortional initial geometric imperfection (0G+1D) provides the lower ultimate load. For columns with intermediate slenderness, controlled in the present study by the variation of the yield stress, the combined initial geometric imperfection with 50% of global and 50% of distortional mode (0.5G+0.5D) gives the lower ultimate load. While for columns with very high yielding, the most detrimental ultimate load takes place with only global initial geometric imperfection (1G+0D). In conclusion, this analysis has shown that the initial geometric imperfection may affect the ultimate load and the column strength in different manners, according to the nature of D-G buckling interaction.

Finally, concerning the nature interaction of the DG coupled phenomenon, some remarks are noted:

(i) It has been noticed that for high yield strength columns in secondary-global bifurcation DG buckling interaction region (which means lower values of $R_{\lambda GD}$) appears to diverge from the original direct strength method, which indicates an evidence of DG buckling interaction;

(ii) Comparing the results with the two types of initial geometric imperfection considered (0.5G+0.5D and 1G+0D), it was concluded that the influence of the initial geometric imperfection was negligible in the numerical ultimate load. Thereby, using an initial geometric imperfection with only global (flexural-torsional) buckling mode shape is sufficient to perform a parametric study on distortional-flexural-torsional coupled phenomenon;

(iii) Generally speaking, the direct strength method equation addressed to global buckling, Eq. 11, is able to handle quite well the columns under the different D-G nature (of the buckling interaction). However, the limits of the present investigation must be pointed, since only lipped channel columns were considered. Additional results of columns with different cross-section shapes are needed to strengthen this assumption as a general rule;

(iv) The proposed equations by Schafer [30] (Eq. (13)) and Martins et al. [14] (Eq. (14)) addressed somewhat conservative results for the strength of the lipped channel columns described in the present research. More specifically, between the two approaches investigated, the P_{nGD} equation (Eq. (14)) has demonstrated more conservative than the P_{nDG} (Eq. (13)) approach.

The conclusions obtained from the DG buckling interaction behavior are basically aligned with the ones found in and Martins *et al.* [14], Dinis and Camotim [13] and Martins *et al.* [31]. However, more investigations on this topic is still needed. The present research suggests laboratory experiments, in order to better understanding the phenomenon.

9. Acknowledgments

This research was financially supported by CNPq (Proc. 131199/2018-8) and FAPERJ grant E-26/200.825/2019 (242580).

References

[1] E. de M. Batista, “Modelling Buckling Interaction,” in *Phenomenological and Mathematical Modelling of Structural Instabilities*, vol. 470, M. Pignataro and V. Gioncu, Eds. Vienna: Springer Vienna, 2005, pp. 135–194.

[2] ASSOCIAÇÃO BRASILEIRA DE NORMAS TÉCNICAS and ABNT, *NBR 14762 - Dimensionamento de estruturas de aço constituídas por perfis formados a frio*, Segunda. Rio de Janeiro, RJ, Brazil, Brasil: ABNT, 2010.

[3] AS/NZS 4600, *Cold-formed steel structures, Standards Australia & Standard New Zealand*. Australian/New Zealand Standard™, 2018.

[4] AISI S100-16, *North American Specification for the Design of Cold-Formed Steel Structural Members*. American Iron and Steel Institute, 2016.

[5] B. W. Schafer and T. Peköz, “Direct Strength Prediction of Cold-Formed Steel Members Using Numerical Elastic Buckling Solutions,” in *14th International Specialy Conference on Cold-Formed Steel Structures*, 1998, pp. 69–76.

[6] G. J. Hancock, Y. B. Kwon, and E. S. Bernard, “Strength design curves for thin-walled sections undergoing distortional buckling,” *J. Constr. Steel Res.*, vol. 31, no. 2–3, pp. 169–186, Jan. 1994, doi: 10.1016/0143-974X(94)90009-4.

[7] E. de M. Batista, “Effective section method: A general direct method for the design of steel cold-formed members under local-global buckling interaction,” *Thin-Walled Struct.*, vol. 48, no. 4–5, pp. 345–356, 2010, doi: 10.1016/j.tws.2009.11.003.

[8] B. W. Schafer, “Direct Strength Method (DSM) Design Guide,” in *Design Guide CFXX-X, American Iron and Steel Institute*, Committee on Specifications for the Design of Cold-Formed Steel Structural Members, Ed. American Iron and Steel Institute, 2006.

[9] B. W. Schafer, “Review: The Direct Strength Method of cold-formed steel member design,” *J. Constr. Steel Res.*, vol. 64, no. 7–8, pp. 766–778, Jul. 2008, doi: 10.1016/j.jcsr.2008.01.022.

[10] M.-T. Chen, B. Young, A. D. Martins, D. Camotim, and P. B. Dinis, “Experimental investigation on cold-formed steel stiffened lipped channel columns undergoing local-distortional interaction,” *Thin-Walled Struct.*, vol. 150, no. November 2019, p. 106682, May 2020, doi: 10.1016/j.tws.2020.106682.

[11] A. D. Martins, D. Camotim, R. Gonçalves, and P. B. Dinis, “On the mechanics of local-distortional interaction in thin-walled lipped channel columns,” *Thin-Walled Struct.*, 2018, doi: 10.1016/j.tws.2017.12.029.

[12] G. Y. Matsubara, E. de M. Batista, and G. C. Salles, “Lipped channel cold-formed steel columns under local-distortional buckling mode interaction,” *Thin-Walled Struct.*, vol. 137, pp. 251–270, Apr. 2019, doi: 10.1016/j.tws.2018.12.041.

[13] P. B. Dinis and D. Camotim, “Post-buckling behaviour and strength of cold-formed steel lipped channel columns experiencing distortional/global interaction,” *Comput. Struct.*, vol. 89, no. 3–4, pp. 422–434, 2011, doi: 10.1016/j.compstruc.2010.11.015.

[14] A. D. Martins, D. Camotim, and P. B. Dinis, “On the distortional-global interaction in cold-formed steel columns: Relevance, post-buckling behaviour, strength and DSM design,” *J. Constr. Steel Res.*, vol. 145, pp. 449–470, Jun. 2018, doi: 10.1016/j.jcsr.2018.02.031.

[15] E. S. dos Santos, E. de Miranda Batista, and D. Camotim, “Cold-formed steel columns under L-D-G interaction,” *Steel Constr.*, vol. 7, no. 3, pp. 193–198, Sep. 2014, doi: 10.1002/stco.201410034.

[16] G. Y. Matsubara and E. de M. Batista, “Cold-Formed Steel Columns Under Local-Distortional-Global Buckling Mode Interaction,” in *Proceedings of the XL Ibero-Latin-American Congress on Computational Methods in Engineering, ABMEC, Natal, RN, Brazil*, 2019.

[17] S. P. Timoshenko and S. Woinowsky-Krieger, *Theory of Plates and Shells*, no. 2. McGraw-Hill Book Company, Inc, 1959.

[18] Y. K. Cheung, *Finite Strip Method in Structural Analysis*, vol. 3, no. 2. Adelaide: Pergamon Press, 1976.

[19] Y. K. Cheung, “The Finite Strip Method in the Analysis of Elastic Plates with two opposite Simply Supported Ends,” *Proc. Inst. Civ. Eng.*, vol. 40, no. 1, pp. 1–7, 1969, doi: 10.1680/iicep.1969.7550.

[20] Y. K. Cheung, “Finite Strip Method Analysis of Elastic Slabs,” *J. Eng. Mech. Div.*, vol. 94, no. 6, pp. 1365–1378, 1968, [Online]. Available: https://cedb.asce.org/CEDBsearch/record.jsp?dockey=0015652.

[21] M. A. Bradford and M. Azhari, “Buckling of plates with different end conditions using the finite strip method,”

Comput. Struct., vol. 56, no. 1, pp. 75–83, 1995, doi: 10.1016/0045-7949(94)00528-B.

[22] Z. Li and B. W. Schafer, “Finite Strip Stability Solutions for General Boundary Conditions and the Extension of the Constrained Finite Strip Method,” in *Computational Science, Engineering & Technology Series*, no. August 2016, B. H. V. Topping, L. F. Costa Neves, and R. C. Barros, Eds. Madeira, Portugal, 2009, pp. 103–130.

[23] B. W. Schafer, “Chapter 2: Elastic Buckling Solution Methods for Cold-formed Steel Elements and Members,” Ph.D. Thesis, Cornell University, 1998.

[24] Z. Li, “Buckling Analysis of the Finite Strip Method and Theoretical Extension of the Constrained Finite Strip Method for General Boundary Conditions.,” Research Report, Baltimore, MD, 2009. [Online]. Available: http://www.ce.jhu.edu/bschafer.

[25] J. A. de Lazzari, “Distortional-Global Interaction In Cold-Formed Steel Lipped Channel Columns: Buckling Analysis, Structural Behavior And Strength,” Master’s Thesis, Civil Engineering Program, Federal University of Rio de Janeiro, COPPE, 2020.

[26] G. Winter, “Thin-Walled Structures-Theoretical Solutions and Test Results,” 1968, pp. 101–112.

[27] G. Winter, “Strength of thin-walled compression flanges,” *Trans. ASME*, vol. 112, 1947.

[28] ABNT, *Associação Brasileira De Normas Técnicas, NBR 8800:2008 - Projeto de estruturas de aço e de estruturas mistas de aço e concreto de edifícios*. Rio de Janeiro, RJ, Brazil, 2008.

[29] ANSI/AISC 360-16, *American National Standards Institute and American Institute of Steel Construction: Specification for Structural Steel Buildings*. Chicago, Illinois, 2016.

[30] B. W. Schafer, “Local, Distortional, and Euler Buckling of Thin-Walled Columns,” *Journal of Structural Engineering*, vol. 128. pp. 289–299, 2002.

[31] A. D. Martins, D. Camotim, R. Gonçalves, and P. B. Dinis, “On the mechanics of distortional-global interaction in fixed-ended columns,” *Thin-Walled Struct.*, vol. 123, pp. 162–184, Feb. 2018, doi: 10.1016/j.tws.2017.11.001.

[32] MathWorks, “MATLAB Using MATLAB Graphics,” *Matlab*, 2000.

[33] B. W. Schafer, “CUFSM 5.04 - Cross-Section Elastic Buckling Analysis:” Constrained and Unconstrained Finite Strip Method, Baltimore, MD, 2020, [Online]. Available: https://www.ce.jhu.edu/cufsm/downloads/.

[34] R. Bebiano, D. Camotim, and R. Gonçalves, “GBTul 2.0 − A second-generation code for the GBT-based buckling and vibration analysis of thin-walled members,” *Thin-Walled Struct.*, vol. 124, pp. 235–257, Mar. 2018, doi: 10.1016/j.tws.2017.12.002.

[35] ANSYS Inc., *ANSYS Mechanical APDL Theory Reference - Release 15.0*. Canonsburg, PA, 2013.

[36] G. C. de Salles, “Investigação Analítica, Numérica e Experimental do Modo de Flambagem Distorcional em Perfis Formados a Frio,” Dissertação de Mestrado, Universidade Federal do Rio de Janeiro, COPPE, 2017.

[37] E. S. dos Santos, “Interação entre os modos de flambagem local-distorcional-global em perfis de aço formados a frio com seção U enrijecido na compressão axial,” Tese de Doutorado, COPPE/ Universidade Federal do Rio de Janeiro, 2014.

[38] P. B. Dinis and D. Camotim, “Cold-formed steel columns undergoing local-distortional coupling: Behaviour and direct strength prediction against interactive failure,” *Comput. Struct.*, 2015, doi: 10.1016/j.compstruc.2014.09.012.

[39] E. Ellobody and B. Young, “Behavior of Cold-Formed Steel Plain Angle Columns,” *J. Struct. Eng.*, vol. 131, no. 3, pp. 457–466, Mar. 2005, doi: 10.1061/(ASCE)0733-9445(2005)131:3(457).

[40] B. W. Schafer and T. Pekoz, “Computational modeling of cold-formed steel : characterizing geometric imperfections and residual stresses,” *J. Constr. Steel Res. 47*, vol. 47, pp. 193–210, 1998, doi: 0143-974X/98/$19.00.

[41] W. S. Santos, “On the Strength and DSM Design of End-Bolted Cold-Formed Steel Columns Buckling in Distortional Modes,” Tese de Doutorado, COPPE/ Universidade Federal do Rio de Janeiro, 2017.

[42] E. Riks, “An incremental approach to the solution of snapping and buckling problems,” *Int. J. Solids Struct.*, 1979, doi: 10.1016/0020-7683(79)90081-7.

[43] E. Riks, “The application of newton’s method to the problem of elastic stability,” *J. Appl. Mech. Trans. ASME*, 1972, doi: 10.1115/1.3422829.

[44] G. A. Wempner, “Discrete approximations related to nonlinear theories of solids,” *Int. J. Solids Struct.*, 1971, doi: 10.1016/0020-7683(71)90038-2.

[45] Y. B. Heva, “Behaviour and design of cold- formed steel compression members at elevated temperatures,” Thesis, School of Urban Developments Queensland University of Technology, 2009.

[46] J. A. de Lazzari and E. D. M. Batista, “Behavior and Strength of Distortional-Global Interaction in Cold Formed Steel Lipped Channel Columns,” in *Proceedings of the XL Ibero-Latin-American Congress on Computational Methods in Engineering, ABMEC*, 2019, pp. 1–20.